ACCEPTED VERSION

http://hdl.handle.net/2440/79732

Self-assembly of selective interfaces in organic photovoltaics

Scott A. Mauger, Lilian Chang, Stephan Friedrich, Christopher W. Rochester,
David M. Huang, Peng Wang, Adam J. Moulé*

Abstract

The composition of polymer-fullerene blends is a critical parameter for achieving high efficiencies in bulk-heterojunction (BHJ) organic photovoltaics. Achieving the "right" materials distribution is crucial for device optimization as it greatly influences charge-carrier mobility. The effect of the vertical concentration profile of materials in spin-coated BHJs on device properties has stirred particularly vigorous debate. Despite available literature on this subject, the results are often contradictory and inconsistent, likely due to differences in sample preparation and experimental considerations. We attempt to reconcile published results by studying the influence of heating, surface energy, and solvent additives on vertical segregation and doping in polymer-fullerene BHJ organic photovoltaics using neutron reflectometry and near edge x-ray absorption fine structure spectroscopy. We show that surface energies and solvent additives greatly impact heat-induced vertical segregation. We also find that interface charging due to Fermi level mismatch increases PCBM-enrichment at the BHJ-cathode interface. Current-voltage measurements show that self-assembly of interfaces affects the open circuit voltage, resulting in clear changes to the power conversion efficiency.

[*] Prof. A. J. Moulé, S. A. Mauger, L. Chang, C. W. Rochester
Department of Chemical Engineering and Materials Science
University of California
Davis, CA 95616, USA
E-mail: amoule@ucdavis.edu
   Dr. S. Friedrich
Advanced Detector Group
Lawrence Livermore National Laboratory
Livermore, CA 94550, USA
   Dr. D. M. Huang
School of Chemistry and Physics
The University of Adelaide
SA 5005, Australia
   Dr. P. Wang
Manuel Lujan Neutron Scattering Center
Los Alamos National Laboratory
Los Alamos, NM 87545, USA

1 Introduction

The photo-active layer of polymer-based organic photovoltaic (OPV) devices is typically a bulk heterojunction (BHJ), in which a polymer electron donor and fullerene electron acceptor are cast from a common solution to form a mixed layer. The components form an interpenetrating, phase-separated network that provides a large interfacial area for charge separation and continuous pathways for charge transport.[1, 2] The most studied donor-acceptor system is poly(3-hexylthiophene) (P3HT) and (6,6)-phenyl-C_{61}-butyric acid methyl ester (PCBM). Initial research showed that the nanoscale morphology of the BHJ plays a critical role in the efficiency of OPV devices.[3] As a result, much of the subsequent research on P3HT:PCBM BHJs focused on how processing conditions such as casting solvent, deposition method, annealing method, and drying rate could be used to tune the morphology to maximize efficiency.[3, 4]

More recently, the focus has shifted to questions about how the concentration of P3HT and PCBM changes as a function of depth within the BHJ. Polymer-fullerene blends have been shown to vertically segregate due to limited miscibility and interactions with adjacent layers. There are a variety of techniques that have been used measure composition of materials as a function of depth, henceforth referred to as the vertical concentration profile (VCP). In P3HT:PCBM films spectroscopic ellipsometry (SE) [5, 6], dynamic secondary ion mass spectroscopy (DSIMS)[7–9], x-ray photoelectron spectroscopy (XPS)[10, 11], near edge x-ray absorption fine structure spectroscopy (NEXAFS)[6, 9, 12], x-ray reflectometry (XRR)[13], and neutron reflectometry (NR)[14–17] have been used to measure VCP. Electron tomography has also been used to study the three-dimensional structure of BHJs and concentration profiles of the crystallinity of P3HT have be obtained [18], but to our knowledge this technique has not been used to generate a more general VCP. Each of these techniques mentioned above has its own set of advantages and disadvantages that must be considered when trying to determine the VCP of the

BHJ.

SE is attractive because measurements are non-destructive and can be made easily in-house, but it has several drawbacks. First, SE requires models of refractive indexes of the pristine materials, which is complicated for P3HT due its anisotropy.[19] Furthermore, the refractive index of P3HT is highly dependent on the ordering of the chains, so assumptions must be made as to how the refractive index will change as a function of PCBM concentration.[20] SE is also not well suited for this system because the contrast between P3HT and PCBM is small. Finally, it is not possible to perform SE measurements underneath a metal capping electrode.

In comparison, DSMIS has advantages over SE because the contrast is very high due to the ability to measure unique mass signals from P3HT and PCBM and since DSIMS measures concentration, it is not sensitive to the anisotropy or ordering of P3HT.[7] However, the limitation of DSIMS is its depth resolution of approximately 10 nm.[7] Furthermore, P3HT and PCBM have different evaporation rates, which imposes further limits on depth resolution.[9] Finally, DSMIS is a destructive technique due to the sputtering process, so samples cannot be re-measured.

X-rays can also be used to measure the VCP, either through XPS or NEXAFS. Both methods allow for direct measurement of the concentration of components from the peak intensities of the measured elements. The shortcoming of these techniques is that they are surface sensitive. Thus, in order to measure at different depths material must be removed, which is not desirable. One method of removal is ion sputtering, but due to different etch rates of BHJ materials it may cause artifacts.[10] Etching can also be used to remove material and expose buried areas, but it is possible that the etching process will alter the layer which is desired to be left intact. Interfaces can also be exposed using delamination methods, but in some cases some of the removed layer remains after delamination.[10] Concentration vs. depth information can be extracted from x-ray spectroscopy methods by varying the excitation energy (P3HT absorbs more strongly at 245 eV than PCBM) and/or incidence angle.[12] This data relates concentration and depth, but is not quantitative. Finally, it is not possible to perform XPS or NEXAFS measurements underneath a thick metal capping electrode, limiting these techniques to uncapped samples.

Reflectometry techniques are nondestructive and unlike SE, neither XRR or NR are sensitive to polymer anisotropy. XRR is attractive because beam intensity is high, which allows for short measurement times. Unfortunately, the contrast between P3HT and PCBM is low due to similarities in electron density. For NR, the situation is reversed; contrast between P3HT and PCBM is high due

to the low concentration of H atoms in PCBM[14, 15, 21], but neutron beams have low intensities, which result in long measurement times. Another positive aspect of NR is that it can be used to measure samples with a metal capping layer because neutrons are only scattered by nuclei which have similar scattering cross-sections for the entire periodic table.[22] Also, it is possible to detect features with very small length scales. Researchers have been able to measures features as small as 13 Å using NR.[23] However, this is dependent on sample quality and contrast variations within the sample.

There are several factors that may potentially influence the VCP of the BHJ: casting solvent, solvent additives, the surfaces in contact with the BHJ, layer thickness, and solvent/thermal annealing. In an effort to better understand how these factors affect the VCP of P3HT/PCBM BHJs the results of previous studies are summarized in **Table 1** and the sample processing conditions are included. From this table it can be seen that the reported VCP results are quite inconsistent, with reported PCBM concentrations ranging from 0-72% at the top surface and 12-90% at the substrate interface. For all of the unannealed samples, the concentration of PCBM at the top surface is low. This is because a skin of P3HT forms at the air interface during spin coating of the active layer. The interfacial free energy is minimized if P3HT, which has a lower surface tension than PCBM, predominates at this interface. The surface energy of the substrate also controls the concentration of PCBM at the bottom interface. For samples in which the substrate has a moderately high surface energy (SiO_2, glass, or PEDOT:PSS), PCBM is attracted to the interface and has high concentration. In contrast, the P3HT concentration is higher when cast onto a low surface energy substrate, as reported by Campoy-Quilles *et al.*[5] and Germack *et al.*[6]. The data also indicates that the equilibrium concentration at the substrate is achieved during coating as thermal and solvent annealing do not result in significant changes in PCBM concentration at the substrate interface. It is equally apparent that solvent and thermal annealing cause changes in the concentration of PCBM at the top surface and in the middle of the BHJ.[10] It should be noted, however, that the effect of annealing on the PCBM concentration at top interface of the BHJ gives inconsistent results. Some reports show heating leads to an increase in the PCBM concentration[10, 15], while in other cases, the PCBM concentration is shown to decrease [9, 10, 14]. Also, the role of casting solvent is not clear. For the majority of previous studies, chlorobenzene is used as the casting solvent and the results are in good agreement. But Germack *et al.*[6] and Xu *et al.*[10] use 1,2-dicholorobenzene and report differing VCP after solvent annealing. Compared to the samples cast from chlorobenzene, Germack *et al.*[6] report a very high concentration of PCBM at the bottom sur-

face (81% measured using SE and 90% with NEXAFS), whereas Xu et al.[10] report a low concentration of PCBM (55-58% with XPS) at the same interface. Germack et al. solvent annealed their samples after spin coating, but for the samples cast from chlorobenzene, solvent annealing was shown to cause little change in the bottom concentration of PCBM. The surface energies of the substrates used in the studies should be comparable between studies since the BHJs were cast onto either quartz or SiO_2. While all of these studies lay a solid foundation in the investigation of the factors controlling the VCP of P3HT/PCBM BHJs, there are clearly still questions to be answered.

One question is: what is the role of the metal electrode? Results from Orimo et al. shown in Table 1 show that heating the BHJ after the deposition of an Al electrode results in an enrichment of PCBM at the top of the BHJ compared to a BHJ that was heated prior to Al deposition.[11] This result was confirmed using DSIMS and NEXAFS in a subsequent study, and PCBM enrichment is shown to occur for very short heating times.[9] What is not clear from these studies is whether this enrichment is a universal trend for samples heated with an intact metal electrode or whether it is unique to an Al electrode. Also, a potential issue with these studies is that the measurements were made after the Al electrode was removed. It is possible that the electrode removal process also removes a portion of the BHJ or provides local heating that changes the interface concentration ratio and casts doubt on the generality of the results.

Another question that has not been answered is: what effects do solvent additives have on the VCP? It is common to add small concentrations of secondary solvents or additives to the casting solution in an effort to improve the efficiency of OPV devices.[24] The additives result in the formation of aggregated domains upon casting, which have small length scales and result in a well mixed nanostructure. These domains are often interpenetrating, and because they form during casting the electrical contact is good, resulting in good charge transport and charge collection efficiency. It is not known how these additives affect the thermal stability of the BHJ. When nitrobenzene is used as an additive, the device properties of an as-cast and heated samples are almost identical, indicating that the electrical properties of the device do not change significantly with heating.[25] Thermal stability of morphology is an important property to consider because OPV devices need to be able to withstand temperature cycles due to daily changes in illumination and seasonal weather. For these reasons, we focus on samples that are cured using nitrobenzene so that we can more easily compare IV and morphology measurements between annealed and unannealed samples.

In this study, we answer these two questions. First, we use NR to study how different metals and solvent additives affect the VCP of P3HT/PCBM BHJs. Since we are using NR, we are able to measure the VCP of a BHJ under an intact metal electrode, which allows us to avoid any possible artifacts introduced by electrode removal. Next, we use NEXAFS spectroscopy to determine the element-specific bonding structure in PCBM films capped with thin metal layers. These measurements are possible because the 2-nm metal capping layer is thinner than the Auger electron escape depth. Finally, we connect our findings on the materials distribution in the BHJ and the chemistry at the BHJ–metal interface to device performance and PCBM aggregate formation. We show here that a capping metal electrode has a profound influence on the VCP. In particular, the VCP changes drastically upon mild heating of the BHJ layer due to interactions with the capping layer. Thus, any conclusion about device performance that have been based on the VCP of an initially uncapped BHJ layer must be treated with caution. We show that solvent additives affect the VCP and that nitrobenzene in particular improves the thermal stability of the BHJ morphology. Finally, we show that low work function capping metals will donate electrons to PCBM through interface charge-transfer and exohedral doping and that this charging of the PCBM contributes to the final VCP of the BHJ, and thereby to the JV characteristics.

2 Results and Discussion

2.1 Measurement of Materials Distribution

To determine the effect of the metal electrode on the VCP in the active layer, NR measurements were performed on P3HT:PCBM BHJ (1:1 weight ratio) samples cast from chlorobenzene/nitrobenzene (2%) with Ag or Al electrodes (henceforth referred to as Ag-capped and Al-capped, respectively) before and after heating at 150°C for 5 min. The samples were cast on Si wafers, even though this geometry does not exactly represent a functional device. We note that this difference does significantly affect our results. Using NR, Kiel et al. found that the profile of P3HT:PCBM BHJs cast on Si or PEDOT:PSS are similar.[14] In addition, we have previously published NR studies on P3HT:PCBM blends on PEDOT:PSS and find that the profiles obtained for those samples are similar to those obtained for this study.[17] **Figure 1**a and b shows the measured reflectivity spectra for the Ag- and Al-capped samples, which were fit using a slab model for the scattering length density (SLD) of the film. When fitting, the SLD of the metals, silicon, and native oxide were fixed at the values found using the NIST SLD calculator to decrease the number of fitting parameters and reduce correlations.[27] The BHJ was represented using 3 to 4 layers, depending on the sample. This simple model of the BHJ proved to be more useful than

Table 1: Summary of published results of concentration of PCBM within P3HT/PCBM BHJs. Values are reported as a function of measurement technique, casting solvent, treatment (solvent or thermal annealing), and top and bottom surface. PCBM concentration values are reported at the top, middle, and bottom surface. PCBM concentration values are reported at the top, middle, and bottom of the BHJ.

Ref #	technique	casting solvent	bottom surface	top surface	treatment	% PCBM top	% PCBM middle	% PCBM bottom	additional comments
[5]	SE	CB	quartz	air	as-cast	25[a]	63[a]	75[a]	
			quartz	air	heated	50[a]	45[a]	74[a]	annealing temperature 140°C
			PEDOT:PSS	air	as-cast	25[a]	50[a]	65[a]	
			PEDOT:PSS	air	heated	50[a]	45[a]	74[a]	annealing temperature 140°C
			quartz	air	as-cast	15[a]	63[a]	75[a]	5000 rpm
			quartz	air	as-cast	32[a]	60[a]	75[a]	3000 rpm
			quartz	air	as-cast	35[a]	50[a]	75[a]	700 rpm
			hydrophobic SAM	air	as-cast	20[a]	48[a]	5[a]	SAM: hexamethyldisilazane
			quartz	air	solvent	62[a]	45[a]	73[a]	solvent annealed for 1 hr
[10]	XPS	DCB	glass	air	as-cast	35		55	3000 rpm
			glass	air	heated	25		49	3000 rpm, 110°C 10 min
			glass	air	as-cast	36		58	800 rpm
			glass	air	heated	36		60	800 rpm, 110°C 10 min
[11]	XPS	CB	PEDOT:PSS	air	heated	36			150°C 30 min
				Al		72			
	SE	DCB	SiO$_2$		solvent	0	41	81	
			PEDOT:PSS	air	solvent	0	41	54	
			PTT/Nafion		solvent	0	43	12	
[6]			SiO$_2$			26		90	20 min solvent anneal
	NEXAFS	DCB	PEDOT:PSS	air	solvent	26			
			PTT/Nafion		solvent	26		20	
[9]	NEXAFS	CB	PEDOT:PSS	air	as-cast	12			
				air	heated	8			
				Al	heated	41			5 sec, 150°C
						44			1 min, 150°C
						61			30 min, 150°C
[15]	NR	CB	SiO$_2$	air	as-cast	15	30	75	1:0.7 P3HT:PCBM mass ratio
					solvent	15	30	75	solvent annealed 5 min
					solvent + thermal	30	30	75	solvent annealed 5 min + 150°C 1 hr
[14]	NR	CB	SiO$_2$	air	as-cast	28	50[a]	70	800 rpm
					as-cast	37	50[a]	65	2500 rpm
					heated	32[a]	45[a]	75[a]	2500 rpm, 140°C
[26]	NEXAFS	CB	glass	air	as-cast	97		65	film delaminated, 165°C 30 min

[a] Value read from graph

Figure 1: Neutron reflectometry of metal-capped P3HT:PCBM bulk heterojunctions. Reflectivity spectra with fits for P3HT:PCBM BHJs with metal electrodes: (a) Ag, as-cast (■) and Ag, heated (●); (b) Al, as-cast (▲) and Al, heated (♦). The reflectivity profile generated from the fit (—) to the data is included for each sample. Spectra are offset for clarity. Modeled scattering length density profiles for the (c) Ag, as-cast (—) and Ag,heated (– – –) and (d) Al, as-cast (– · –) and Al, heated (– · · –) Depth increases from the substrate interface (0 nm) to the metal/air interface.

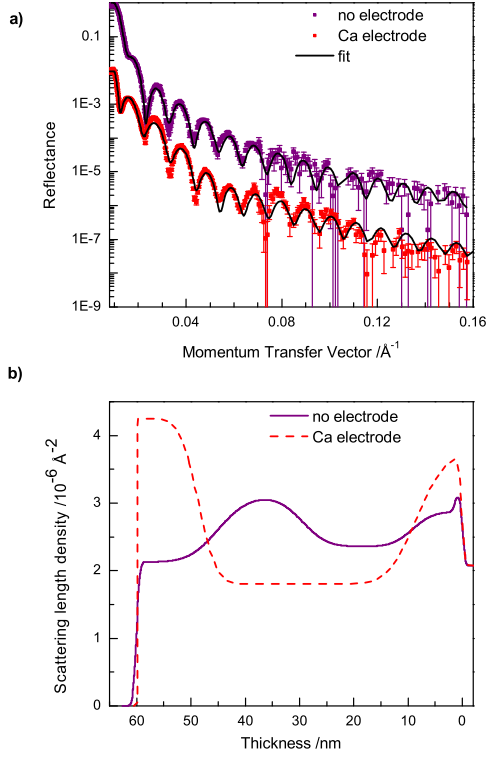**Figure 2:** Neutron reflectometry of P3HT:PCBM bulk hetero-junctions cast from chlorobenzene heated with (BHJ + Ca) and without (BHJ) a Ca electrode. The Ca layer was removed prior to measurement. a) Reflectivity spectra from the annealed un-capped BHJ (■) and Ca-capped (BHJ + Ca, •) samples with best fit reflectivity data (—). Spectra are offset for clarity b) Modeled scattering length density profile for the BHJ (—) and BHJ + Ca (– – –).

more complex models (10 or more layers) as the complex models produced oscillatory profiles that were not physically relevant. The resultant SLD profiles as a function of sample thickness d are shown in Figure 1c and d, where $d = 0$ nm corresponds to the Si substrate. At the top of each sample the profiles show the Al and Ag layers. The top surface roughness of the samples and surface roughness with the metal layer removed were measured using atomic force microscopy and are consistent with the the values obtained from fitting the NR data. In the BHJ, high SLD values correspond to a high concentration of PCBM. The SLD profiles for the BHJ regions of the as-cast samples are very similar. At $d = \sim$67 nm and $\sim$58 nm for the Al-capped and Ag-capped samples, respectively, there is a dip in the SLD, corresponding to the P3HT-rich skin formed during spin coating. This is consistent with previous studies of VCP reported in Table 1. The thickness of these skins are less than 3 nm, which is hard to resolve given the measured range of the momentum transfer vector (Q). To asses the significance of these skin layers, the quality of the fits were compared to models without a layer accounting for the P3HT skin. When a layer was included to account for the skin, the χ^2 values for the Ag- and Al-capped samples were 9.3 and 10.9, respectively. When this skin layer was removed, the χ^2 values increased to 23.7 and 16.4. This shows the significance the skin layer and validates its inclusion in the slab models. Beneath the P3HT skin is a region of increased SLD due to PCBM enrichment. Finally, the bottom 20 nm of the the BHJ shows an increase in SLD, which is almost identical between the two samples. The high SLD is due to PCBM enrichment at the Si/SiO$_2$ due to the high surface energy of the oxide.[6]

Polymer:fullerene solar cells are often annealed to improve device performance.[28, 29] Samples are typically heated to 150°C, which is above the glass transition temperature (T_g) of the mixture.[30] With heating, the P3HT and PCBM distributions change as the system tries to minimize free energy. After heating, there is an increase in SLD at the metal interfaces due to PCBM enrichment and *no indication of the P3HT-rich skin*. Since this occurs in both samples, it indicates that PCBM enrichment is a result of heating with an intact cathode and is not unique to Al. Unlike the as-cast samples, which had very similar VCP for the BHJs, we see that there are significant differences between the profiles of the annealed Ag- and Al-capped samples (can also be seen in raw reflectance data). The differences between the samples clearly shows that the type of metal electrode influences phase segregation throughout much of the BHJ, not just at the surface. For the heated Al-capped sample, the spike in SLD at $\sim$80 nm corresponds to the growth of an aluminum oxide layer that formed during heating. This layer complicated fitting the reflectivity spectrum because it resulted in significant at-

tenuation of the fringes at moderate values of the momentum transfer vector. This sample was also measured using SE to confirm the thickness of the Al_2O_3 layer. The thicknesses for the oxide and Al obtained through ellipsometry are consistent with those obtained from the fit to the NR data. Since the fringes are attenuated, in order to asses whether the interfacial roughness of the BHJ, Al, and oxide are indeed the best fit we did a systematic study. The thickness of the interfacial roughness of the BHJ was increased from the value that produced the best fit, 0.5 Å, to 20 Å. This value was fixed and the interfacial roughnesses of the Al and oxide were fitted along with the thickness of the layers. The resulting roughness and χ^2 values are reported in Table S1. We find that increasing the thickness of the interfacial roughness increases χ^2. It can also be seen that the thicknesses of the other roughness values do not change appreciably as the roughness of the BHJ is changed indicating that they are indeed correct. At the substrate interface, the thickness and SLD of the PCBM-rich region does not appreciably change for either sample, again, consistent with prior results. Another indication of the accuracy of the fits is that for both the Al- and Ag-capped samples the thicknesses of the BHJ is the same before and after heating.

We also used NR to measure a P3HT:PCBM BHJ film cast from pure chlorobenzene, heated with and without a Ca electrode. These samples differ from the heated Al-capped and Ag-capped samples in two ways: 1) they were cast without a high boiling temperature solvent additive (nitrobenzene) and 2) the metal was removed prior to measurement for the Ca-capped sample. The Ca was washed off with water prior to measurement because Ca is quickly oxidized by air, which would create a mixed Ca/CaO layer with unpredictable thickness and SLD, which would significantly decrease measurement accuracy. The NR spectra with fits and modeled SLD profile are shown in Fig 2. Like the heated Al- and Ag-capped samples, the Ca-capped sample has high SLDs at both interfaces indicating PCBM enrichment. In contrast to the samples annealed with electrodes, the heated, uncapped sample shows much reduced vertical segregation and air interface rich in P3HT. The differences between Ca-capped and uncapped samples clearly show that the metal electrode influences phase segregation throughout the entire BHJ. As a consequence, measurements on BHJ samples heated without a cathode *are not representative of an actual device*. Prior measurements of PCBM diffusion indicate that diffusion can occur at 50°C, which is within the normal PV operating range.[7]

2.2 Connecting processing history to performance

To help relate the SLD profile of the BHJ to device performance we converted it to the corresponding PCBM volume percentage within the BHJ. The volume percent PCBM (V_{PCBM}) was calculated using

$$V_{PCBM} = \frac{\rho(z) - \rho_{P3HT}}{\rho_{PCBM} - \rho_{P3HT}}, \qquad (1)$$

where $\rho(z)$ is the SLD at a depth z, ρ_{P3HT} is the SLD for pure P3HT, and ρ_{PCBM} is SLD for pure PCBM.

The VCP is shown as a function of the normalized depth of the BHJ layer in Fig. 3a–c for the Ca-, Al-, and Ag-capped samples, respectively. For all samples, the average PCBM concentration was calculated to be 44–48 vol%, which is consistent with the average concentration of 46 vol% based on the casting solution. The PCBM concentrations at the top, middle, and bottom of the BHJ for each of the samples are summarized in **Table 2**

The as-cast Al- and Ag-capped samples have similar VCPs, because the BHJ morphology at room temperature is essentially fixed since the P3HT/PCBM mixture is below its T_g and should not be substantially altered by deposition of the metal electrode. The concentration of PCBM at the bottom of the BHJ is 61-63 vol%. This value is lower than what is more commonly reported ($\sim$75 vol% [5, 14, 15]) likely due to the addition of nitrobenzene to the casting solvent for our samples. This concentration does not change with heating, which is consistent with many of the other studies[5, 10, 15].

Interpretation of the data at the metal interface is significantly more difficult. The as-cast PCBM concentration at the metal interface is initially low, 45 vol% for Ag and 14 vol% for Al. But it is not clear why the two concentrations differ for as-cast layers. The difference between these two values is likely influenced by roughness with the capping metal leading to smearing of the interface. The P3HT skin layer is also quite thin and is barely resolvable in the available Q-range of the NR data. If we assume no influence on the SLD from the metal, then the concentration of PCBM at the Ag-BHJ interface increases from 45 vol% to 72 vol%. For the Al-capped sample, the PCBM concentration at the metal interface increases from 14% to 47 vol% with annealing. This result is consistent with NEXAFS measurements of samples that were heated for similar lengths of time.[9]. For both samples the apparent change in concentration at the metal interfaces is an increase of 30 vol% PCBM. Can these results be reconciled? In the Ag-capped sample, Ag has a high SLD (3.47), so in an assumed mixture with the BHJ it will increase the overall SLD near the interface. In contrast, Al has a much lower SLD (2.08), so it will not have as much of an effect on the overall SLD as Ag does. Without *a*
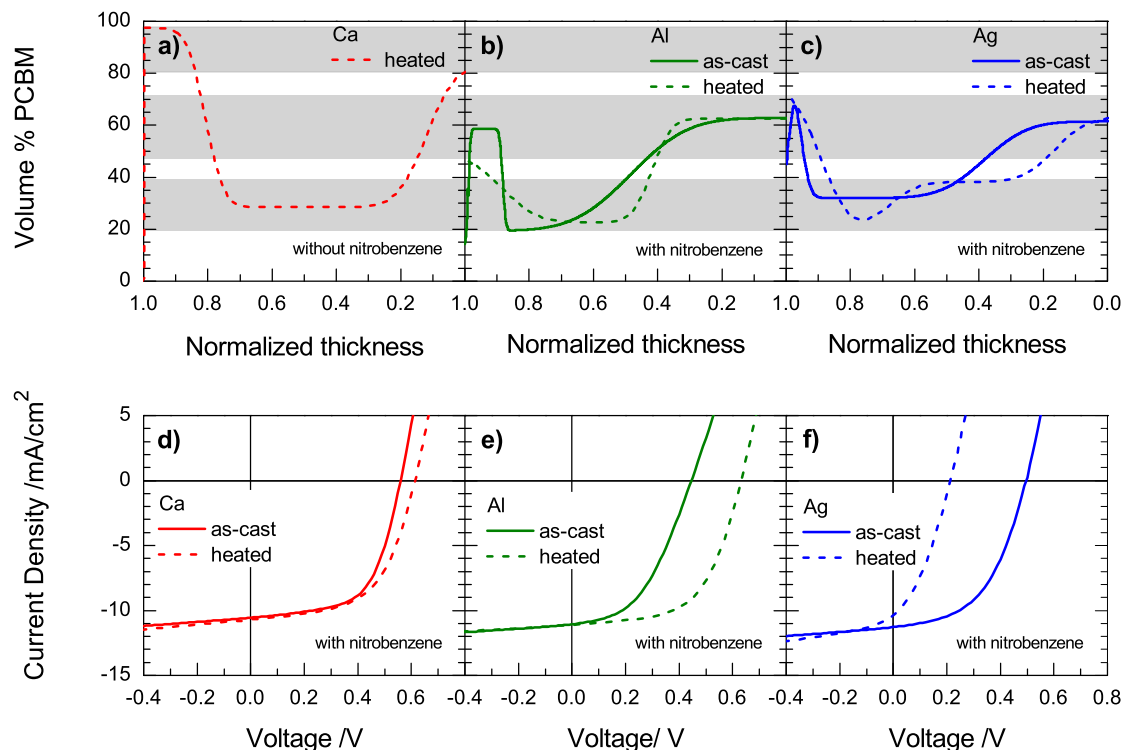
Figure 3: Current density-voltage measurements and vertical concentration profile of P3HT:PCBM devices. **a-c** PCBM volume percent as a function of normalized depth in the BHJ for as-cast and heated samples capped with metal layers: **a)** Ca (as-cast —, heated – – –), **b)** Al (as-cast —, heated – – –), and **c)** Ag (as-cast —, heated – – –).The shaded regions indicate the three different concentration ranges. The region from 20–38 vol% is the eutectic/metastable region. 47–73 vol% is the PCBM concentration when limited due to the use of nitrobenzene. 80–98 vol% is the maximum concentration of PCBM when there are no solvent additives. **d-f** Current-voltage curves for P3HT:PCBM OPV devices with different cathode metals: **d)** Ca, **e)** Al, and **f)** Ag. Devices were measured as-cast and after heating at 150 °C. P3HT:PCBM BHJ were cast from a solution of chlorobenzene with 2% nitrobenzene to fix the BHJ morphology. Devices were measured under 1 Sun of simulated AM 1.5G light with no mismatch correction.

Table 2: PCBM volume concentration for P3HT:PCBM BHJ samples measured with neutron reflectometry. Values are reported for the top, middle (50% of normalized depth), and bottom of the BHJ layer. The BHJs were cast from pure chlorobenzene (CB) or a mix of chlorobenzene and nitrobenzene (NB). All heated samples were heated at 150°C for 5 min.

casting solvent	top surface	treatment	% PCBM top	% PCBM middle	% PCBM bottom
CB/NB	Ag	as-cast	45	35	61
		heated	72	38	63
	Al	as-cast	14	39	63
		heated	47	24	63
CB	air	heated	38	56	55
	Ca		97	29	80

Table 3: Device parameters for P3HT:PCBM OPV devices. Open-circuit voltage (V_{OC}), short-circuit current (J_{SC}), fill factor (FF), and power conversion efficiency (PCE) for P3HT:PCBM devices with different metal electrodes measured as-cast and following annealing at 150°C. Devices were measured under simulated 1 Sun AM 1.5G light with no mismatch factor.

		V_{OC} (V)	J_{SC} (mA/cm^2)	FF	PCE (%)
Al	as-cast	0.45	11.06	0.45	2.08
	heated	0.63	11.10	0.58	3.77
Ag	as-cast	0.50	11.28	0.50	2.63
	heated	0.21	10.37	0.35	0.72
Ca	as-cast	0.56	10.56	0.61	3.35
	heated	0.61	10.71	0.57	3.45

priori knowledge of the concentration of one of the three components at the interface, it is not possible to determine the concentrations at the interface, as the problem is under specified. If it is assumed that the concentration of Ag is 25 vol%, then we find that the PCBM concentration at the top of the BHJ is initially 20 vol% and increases to 51% with annealing, which is consistent with the previous studies and is in better agreement with the Al-capped sample. This data and discussion shows that PCBM diffuses to the metal interface and the P3HT skin disappears after heating because the metal interacts more favorably with PCBM than with P3HT, as suggested by the higher surface energy γ of PCBM [31] compared with P3HT[32]. This behavior is *opposite* to that expected at an air interface, where free energy is minimized by a predominance of the lower surface-energy P3HT. Finally, even using NR, it is not possible to unequivocally assign concentration profiles at hetero-interfaces due to roughness effects. This data may reveal that the metal mixes more with the BHJ material than previously assumed.

For the heated-Ca-capped and heated-uncapped samples, which were cast without nitrobenzene, the VCPs are very different. The Ca-capped sample has a PCBM concentration of 97 vol% at the top of the BHJ. At the bottom of the BHJ the PCBM concentration is 80 vol%, which is in agreement with previous results.[5, 6, 14, 15] As was the case for the heated Ag- and Al-capped samples, there is no P3HT-rich top surface. The uncapped sample is P3HT-rich at the interface, with a PCBM concentration of 38 vol%, which is consistent with previous measurements of BHJs that were heated uncapped.[10, 11, 14, 15]

Despite large differences between the VCPs of heated and unheated samples, all samples have a constant PCBM concentration in the center, or bulk, of the layer of ∼24–40 vol% PCBM, which is consistent with the eutectic point and metastable regions for published P3HT:PCBM

phase diagrams.[33, 34] This concentration is also observed in solution-cast bi-layers and BHJ cast onto PEDOT:PSS.[7, 9, 17] It is also worthy of note that although the metal does substantially affect the VCP, the magnitude of the surface energy of the metal (γ = 0.5 J/m^2, 1.15, and 1.25 J/m^2 respectively for Ca, Al, and Ag [35]) does not appear to be an important factor. Fig. 3a–c and Table 2 show that the PCBM concentration is below 75 vol% at metal interfaces for both the Al- and Ag-capped samples while it is >95 vol% in the Ca-capped sample at both interfaces, whereas surface energy considerations would predict a lower PCBM concentration at the lower surface-energy Ca interface.

Instead, the measured VCPs suggest that the interfacial PCBM concentration at the interfaces is strongly affected by the presence of the solvent additive, nitrobenzene, which was used in casting the Al- and Ag-capped samples, but not in the Ca-capped sample. The concentration of PCBM at the metal and substrate interfaces is higher in the Ca-capped sample than in the Al- and Ag-capped samples. Nitrobenzene has been shown to reduce the diffusion rate of PCBM in P3HT, to increase the T_g of the BHJ mixture, increase P3HT crystallinity, and cause the formation of larger P3HT and PCBM domains.[25, 36] Fig. 4 presents a schematic to highlight the differences between BHJs cast with and without nitrobenzene. Our interpretation of the interface concentration is as follows. When the samples are cast, the interface is rich in P3HT due to the skin that forms upon coating. Just below this skin, the PCBM concentration is above its solubility limit in P3HT and pure domains form. With heating above T_g PCBM diffuses to the interface to minimize the free energy of the surface. When nitrobenzene is added to the casting solvent (Ag- and Al-capped) the total concentration of PCBM is limited to below 70 vol% because of the high number of pre-formed P3HT aggregates restrict PCBM diffusion and PCBM molecules can only occupy space between the aggregated P3HT domains that form during casting. In contrast, when there is no solvent additive (Ca-capped), the BHJ layer is initially much less crystalline, as shown in Fig. 4. Heating allows PCBM diffusion towards the interfaces but there are fewer pre-formed P3HT fibers to limit diffusion so an almost pure PCBM layer can form at the electrode. As mentioned above, the concentration of the PCBM-enriched region at the substrate surface also indicates that the PCBM concentration is controlled by the presence of nitrobenzene as the concentration of PCBM at the SiO$_2$ interface is much higher in the Ca-capped sample than for the Ag- and Al-capped samples.

But surface energy effects and solvent additives clearly are not the only contributors to changes in vertical segregation with heating. If we consider the thickness of the PCBM-enriched layer at the metal interface, it is clear
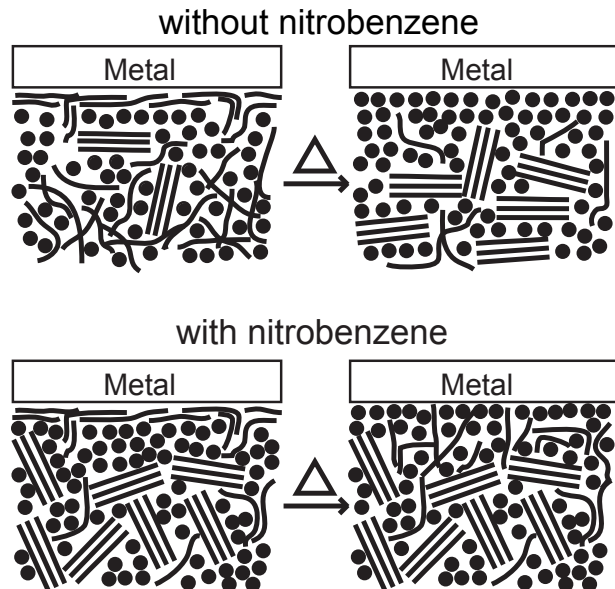
Figure 4: Schematic comparing the vertical concentration profile of P3HT:PCBM BHJ devices cast with and without the solvent additive nitrobenzene before and after heating. Note that the effects of charging by the metal are not included.
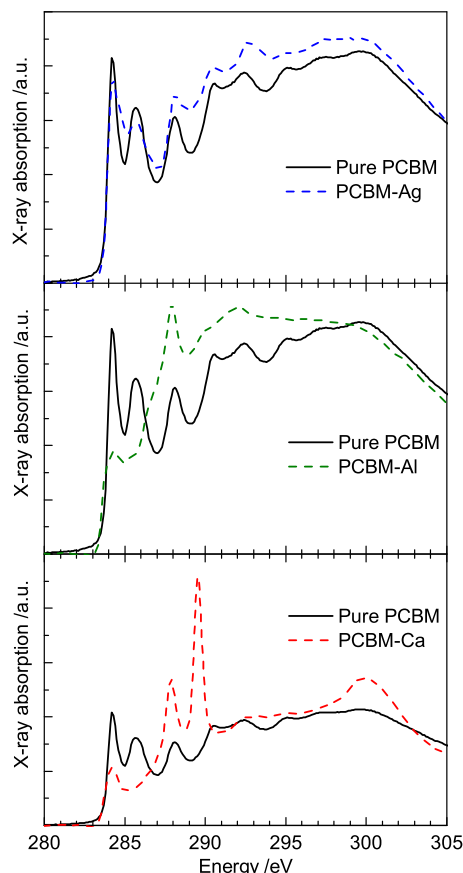

Figure 5: Carbon K-edge x-ray absorption of metal capped PCBM samples. NEXAFS spectra measured in total electron yield for the pure PCBM (—) and PCBM capped with **a)** Ag (– – –), **b)** Al (– – –), and **c)** Ca (– – –). Samples were heated to 150 °C for 10 min prior to measurement.

that Ca and Al have thick PCBM-rich layers (∼20% of total thickness) whereas the Ag-capped device has a thinner PCBM-enriched layer (∼10%) followed by a PCBM-depleted layer (∼10%).

2.3 Interfacial Charging

Another possible contributor to the large change in VCP that occurs with heating is a specific chemical/physical interaction between the metal and BHJ materials. To determine what interactions are present, we have used NEXAFS spectroscopy to probe element-specific bonding. Because the VCP data indicated an increased PCBM concentration near the metal interface, experiments were performed on heated samples with metals and PCBM only to simplify data interpretation.

To determine the effects that the electrode material may have on the carbon chemistry of PCBM, NEXAFS spectra by total electron yield (TEY) are taken on the carbon K-edge for a pure PCBM reference and for PCBM films under thin metal electrodes. The spectra in Fig. 5 of pure PCBM is consistent with previously publshed NEXAFS spectra of PCBM.[9, 12, 37, 38] The first two peaks at 284.2 eV and 285.8 eV correspond to the π^* transitions and those above 292 eV σ^* transitions of PCBM.[12] There are no significant differences between the pure PCBM and PCBM–Ag spectra aside from a slight peak broadening due to the stress induced by the Ag overlayer. In contrast, the PCBM–Al and PCBM–Ca spectra dif-

fer significantly from pure PCBM, indicating that PCBM has undergone chemical changes. Most importantly, the first two π^* peaks in both spectra have decreased in amplitude, corresponding to a reduced number of unoccupied states in the lowest unoccupied molecular orbital (LUMO) of PCBM, and indicating that the Al and Ca electrodes are donating electrons to PCBM through either a charge-transfer or doping process. In order for either of these processes to occur, the Fermi level of the metal must be above (closer to the vacuum level) the LUMO of the matrix material.[39] The Fermi levels for the metals used are -2.9 eV, -4.2 eV, and -4.6 eV for Ca, Al, and Ag, respectively.[40] The LUMO of PCBM is -4.3 eV [41]. Since the Fermi levels of Al and Ca are above the LUMO of PCBM these metals should be able to donate electrons to PCBM. This is exactly what is observed in the x-ray spectra. The Fermi level of Ag[40] is lower than the LUMO of PCBM, so electrons do not move from Ag to PCBM.

Both charge transfer to and doping of fullerenes by metals are established phenomena. Charge transfer at the interface between PCBM and Ca or Al has been shown to occur spontaneously.[42] In this process, electrons tunnel across the interface to align the energy levels of the metal and the BHJ. In the bulk doping process, the metal diffuses into the BHJ where it donates an electron(s) to the fullerene, which is easily able to accept the electron(s) because of the unsaturated C–C bonds.[43] This process, known as exohedral doping, results in a bound complex between the metal and the fullerene. To our knowledge exohedral doping has not previously been shown to occur in OPV devices. Since charge transfer occurs spontaneously it is at least partially responsible for the structure of the NEXAFS spectra for the Ca– and Al–capped PCBM. But it is also possible that doping is also occurring in these samples.

To understand what interactions are taking place between the metal and the PCBM we measured the NEXAFS spectra at the Ca L-edge of PCBM samples with Ca electrodes present. With the electrode present, a clear Ca spectrum is observed (Supporting Information, Fig. S1) in total electron yield (TEY), which is surface sensitive. The spectral fine structure, especially the strong pre-edge features at 345.0 and 348.2 eV, indicate Ca oxidation, as expected since it was exposed to atmosphere prior to measurement. The peaks are wider than those of pure commercial CaO and Ca(OH)$_2$ model compounds because oxidation in ambient air produces (hydr)oxides in different configurations with slightly inhomogeneous characteristics. The air stable form of Ca is CaCO$_3$, which is completely unreactive. The NEXAFS scans were repeated on a PCBM sample whose Ca electrode had been washed off (expected product CaCO$_3$). As expected, a scan by TEY shows no structure at the Ca L-edge above the back-

ground, indicating a surface Ca concentration below 1 vol%. A high-resolution superconducting tunnel junction x-ray spectrometer with detection limits as low as 100 ppm[44] was then used to retake the spectrum by partial fluorescence yield (PFY), which is a bulk-sensitive measurement. This spectrum shows a weak Ca signal, indicating the presence of Ca inside the PCBM layer. This was not unexpected, as previous studies have shown that electrode materials can disperse throughout devices.[45, 46] Surprisingly, the pre-edge features at 345.0 and 348.2 eV differed from those of the oxidized Ca electrode, suggesting the presence of Ca in a different chemical state. Comparisons to a CaC$_2$O$_4$ model compound and Ca L-edge spectra in literature indicate that the Ca ion is bound to carbon.[47] This suggests exohedral doping is occurring between Ca and PCBM. The difference in the peak intensities of the Al-capped and Ca-capped NEXAFS spectra indicate that doping and charge transfer are occurring more strongly with Ca than Al. This is to be expected given the difference in Fermi levels of the metals.

Since the NEXAFS data suggests that the metal is diffusing into the BHJ, it may be affecting the crystallinity of PCBM. The crystallinity of PCBM should be reduced if there are metals present in the BHJ as the metal ions will act as defect sites and disrupt formation of extended PCBM crystals. To determine if dissolved metal ions affect PCBM crystallization, we prepared capped, annealed BHJ samples and used reflection optical microscopy to see if there is a difference in the size and number of PCBM crystals. From the images shown in **Figure 6** it can be seen that the Ag-capped sample, heated under identical conditions, has a higher number of visible crystals than the Al- or Ca-capped samples. This confirms the NEXAFS result that the metal is in the BHJ and not just at the surface. It also suggests that doping/charge transfer results in a higher concentration of metal in the BHJ. This may explain why the profile of the heated Ag-capped sample differs from the heated Al- and Ca-capped samples. This data along with the results for NR and NEXAFS suggest that doping/charge transfer and metal diffusion is influencing the VCP. In the Ca– and Al–capped samples where there is doping and charge transfer, the VCP of the heated samples (Fig. 3) do not show a PCBM-depleted region below the PCBM-enriched region at the interface with the metal. In contrast, with Ag, where the data shows no evidence of doping or charge transfer, there is a PCBM-depleted region. This indicates that either the presence of the metal in the BHJ or the charging near the interface is influencing the VCP of the BHJ in annealed samples.
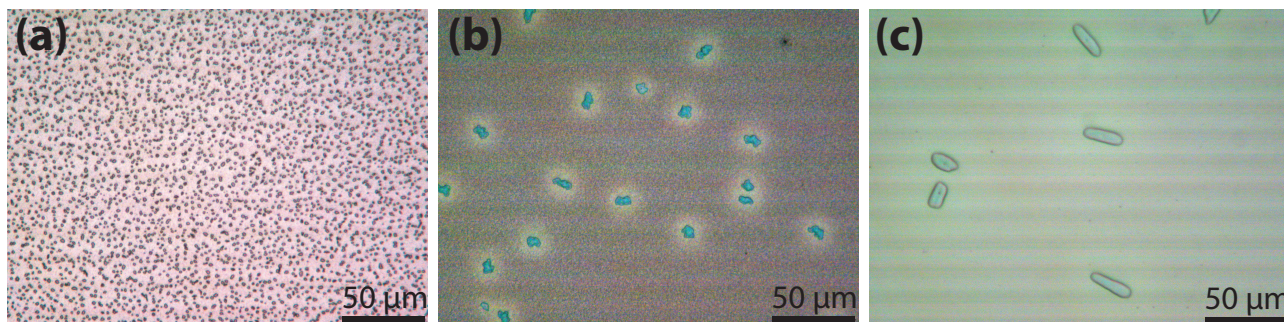
Figure 6: Microscope images of P3HT:PCBM films spin-coated from cholorobenzne/nitrobenzene (4%) and heated at 150°C for 1 hour, capped with a 10 nm layer of **(a)** silver, **(b)** calcium, and **(c)** aluminum.

2.4 Connecting VCP and Doping to OPV device performance

To determine how interface doping/charge transfer and the VCP affect completed BHJ devices, we fabricated P3HT:PCBM OPV devices. The increase in PCBM concentration at the metal electrode should improve device performance by increasing the selectivity for electron-only transport to the metal electrode. It has been shown that a PCBM-rich layer at the anode significantly decreases OPV device efficiency because it blocks holes from being collected at the anode.[26] Based on this result, it is expected that a high concentration of PCBM at the cathode should improve OPV device efficiency because it will block holes from being collected at the cathode. Transistor measurements of P3HT:PCBM films have also shown that the charge-carrier mobility is highly dependent on the ratio of P3HT to PCBM so it is expected that differences in material composition may influence efficiency.[33] Also, the charging of PCBM in the Al-capped and Ca-capped samples should improve efficiency. Devices were fabricated with BHJs cast from chlorobenzene/nitrobenzene solutions, where nitrobenzene was used because it provides a favorable morphology without heating.[25] Note: this choice of samples creates an inconsistency between the Ca-capped sample used for NR measurements and the Ca device because nitrobenzene was not present in the NR measured sample. The reason for nitrobenzene use in the devices is that nitrobenzene causes P3HT crystallization and aggregation of P3HT and PCBM domains during casting. The use of the solvent additive allows us to eliminate crystallization and aggregation as causes for changes in device efficiency that occur with heating. Note that for the Ca device the cathode consisted of 5 nm of Ca and 150 nm of Ag because Ca is easily oxidized. The JV curves of OPV devices with different cathode metals measured before and after heating are shown in Fig. 3d–f and the values of open-circuit voltage (V_{OC}), short-circuit current density

(J_{SC}), fill factor (FF), and power conversion efficiency (PCE) are summarized in Table 3.

Since nitrobenzene was added to the casting solvent, the as-cast BHJ morphology is optimized and thus there are no significant differences in J_{SC} of the as-cast devices.[25] The small differences in J_{SC} are likely due to differences in reflectivity of the cathodes leading to different light intensity distributions in the BHJ.[48] A Ca electrode produces the most efficient devices, because of its low Fermi level, which creates a large built-in potential (V_{BI}) and drives charges to the appropriate electrodes. Additionally, Ca's Fermi level is above the LUMO of PCBM, making it unlikely to accept holes from the HOMO of P3HT. For the Al and Ag devices V_{BI} is smaller due to the higher work functions of the metals. For Ag, its Fermi level is below the LUMO of PCBM, making hole collection at the cathode more favorable than for Ca or Al.

The device data clearly show that heating results in changes in the device electrical properties. With a Ca electrode, PCE improvement upon heating is small, only 3% relatively. Since the Ca electrode is already selective for electrons, the introduction of a hole-blocking, n-doped PCBM-rich layer shown in Fig. 3a does not significantly improve the device, consistent with prior results (see Table 1). There is a small increase in V_{OC} but we believe this is due to an increase in hole selectivity at the anode.[49]

In contrast to the Ca–capped device, heating the Al–capped device improves PCE significantly (∼81%) due to increased V_{OC} and FF. This improvement clearly shows that PCBM enrichment and doping at the cathode improve the selectivity of the cathode for electron collection. The improvement is also consistent with the work of Chen *et al.* who were able showed that heating P3HT/PCBM BHJs with an Al capping electrode resulted in an increase in efficiency, which they attributed to changes in the distribution of materials in the BHJ.[9] Note: we previously published that little change occurs upon annealing for

P3HT/PCBM Al-capped devices with a mixing ratio of 3:2 and nitrobenzene.[**?**] The samples here have a higher PCBM loading of 1:1, which appears to be significant.

The Ag–capped device is affected very differently by heating than the Al– and Ca–capped devices. The VCP in Fig. 3f shows that heating leads to PCBM enrichment at the cathode, but the NEXAFS data shows that PCBM is not doped or charged at the interface. Based on these observations, we expected heating to improve efficiency because of the increased electron selectivity due to the PCBM enrichment at the cathode. However, we observe the opposite result; heating decreases efficiency in Ag-capped devices, mainly due to a 0.3 V drop in V_{OC}. The cause of this decrease in efficiency is the PCBM-depleted region shown in the VCP at a depth of about 0.75 in Fig. 3c. In this region the concentration of PCBM is depleted below its concentration in the rest of the BHJ. Monte Carlo simulations of OPV devices have shown that a depleted region, like this one, commonly forms beneath an enriched region due to the loss of material.[50] This depleted region forms a blocking layer which increases bimolecular recombination. For P3HT:PCBM BHJs bimolecular recombination is known to be a significant loss mechanism, which V_{OC} is dependent upon.[51]

3 Conclusions

Our results show that the metal used as the cathode influences the BHJ in ways not previously known. They dispel the notion that an inverted device architecture is necessary for a favorable material distribution. Rather engineering of the surface energy and electrostatic properties of the interfaces will lead to an idealized vertical concentration profile. We show that the vertical concentration profile is altered by three separate forces. The effect of surface energy has been previously demonstrated. We find that vertical segregation of the BHJ can be reduced with the addition of an additive to the casting solvent. The use of nitrobenzene in the casting solvent reduces the concentration of PCBM at both interfaces by ∼15%.

Additionally, we find that the choice of metal capping electrode affects the vertical concentration profile not only through the surface energy, but also due to the Fermi Energy difference between materials. Low work function metals donate electrons to PCBM through both interfacial charge-transfer and exohedral doping. The presence of charge in the PCBM during annealing affects the final VCP and in turn the IV characteristics of completed OPV devices. This results together show that it is necessary to consider samples processed with intact electrodes for all donor/acceptor pairs to fully understand the relationship between the morphology and device efficiency. Furthermore, the differences in VCP, doping, and device perfor-

mance highlight the sensitivity of OPV devices to sample history. This has broad implications to the organic electronics community, most importantly that comparison of devices with different sample histories may lead to false conclusions due to significant, but unknown differences between samples.

Methods

For neutron reflectometry measurements, silicon wafers were cleaned by rinsing with acetone, isopropyl alcohol, and deionized water, then blow dried with nitrogen, and finally cleaned in a UV/ozone plasma chamber. P3HT and PCBM solutions were prepared by dissolving the polymer (20 mg/ml) or fullerene (20 mg/ml) in chlorobenzene. Nitrobenzene was added at 2% by volume. The solutions were stirred on a hot plate set to 60 °C for 30 minutes. The P3HT and PCBM solutions were mixed together to achieve a 1:1 weight ratio (total solids concentration of 20 mg/ml). The films were deposited via spin coating. Thickness variation over the entire sample area was less than ±2 nm, as verified with a stylus profilometer. The films were not thermally or solvent annealed prior to electrode deposition. Metal electrodes were deposited by thermal evaporation at 0.2 Å/s for the first 5 nm and then the rate was increased to 1.5 Å/s. Neutron reflectometry measurements were performed on the Surface Profile Analysis Reflectometer (SPEAR) at Los Alamos National Laboratory.[23] Measurements were taken in air before and after heating on a hot plate set at 150 °C for 10 minutes. Since the domain sizes that are formed in a P3HT:PCBM BHJ are ∼10 nm[52], the observed scattering length density is representative of the average composition of the layer. For the Ca sample the electrode was washed off using deionized water prior to measurement. The measured reflectivity was fit to a slab model, in which the sample film was assumed to consist of a series of n parallel layers, where layer i has a thickness d_i and constant scattering length density (SLD) ρ_i, sandwiched between super- (air) and subphases (silicon) of infinite extent. Interlayer "roughness" $\sigma_{i,i+1}$, which could include contributions from actual roughness between layers or from interlayer mixing, was accounted for by an error function SLD profile centered at the interface connecting the SLDs of the adjacent layers i and $(i + 1)$. Slab model fitting to the measured data were carried out using the Refl1D software package.[53] The SLDs of air and silicon were taken to be $\rho_{air} = 0$ and $\rho_{Si} = 2.07 \times 10^6$ Å^2, respectively.[27] For the electrodes the SLDs were taken from the NIST SLD database with $\rho_{Al} = 2.08 \times 10^6$ Å^2 and $\rho_{Ag} = 3.47 \times 10^6$ Å^2.[27]For conversion from SLD to volume percent the pure species SLD were $\rho_{P3HT} = 0.786 \times 10^6$ Å^2 and $\rho_{PCBM} = 4.34 \times 10^6$ Å^2. ρ_{P3HT} was de-

termined from previous measurements of pure P3HT on silicon and ρ_{PCBM} is calculated based upon previously reported data for deuterated PCBM.[14]

Spectroscopic ellipsometry measurements were conducted using a VASE model ellipsometer from the J.A. Woollam Co., Inc. and the data was fit within the WVASE32 software package. The data was fit only in the range of 700-1000 nm because in this wavelength range the BHJ is transparent and its refractive index can easily be obtained using a Cauchy dispersion model. For the Al layer, tabulated values of the refractive index of aluminum contained with in the software were used. The thermally grown aluminum oxide was modeled using a Cauchy dispersion model. The tabulated values for stoichiometric aluminum oxide (Al_2O_2) were not used as the SLD of the oxide layer obtained from the NR fits indicates it is not the stoichiometric oxide.

Atomic force microscope measurements of the surfaces of the samples measured by NR were conducted in tapping mode with a Multimode model microscope from Veeco.

For near edge x-ray absorption fine structure measurements, indium-tin oxide (ITO)-coated glass was ultrasonically cleaned in acetone, Mucusol, and deionized water. Next they were sprayed with deionized water and dried with nitrogen in a spin rinse drier followed by UV/ozone plasma cleaning. Samples were fabricated by spin coating a solution of PCBM (20 mg/mL) in 1,2-dichlorobenzene (20 mg/mL) onto the ITO glass. 2 nm of Ag, Al, and Ca were thermally evaporated at a rate of 0.3 Å/s. A pure PCBM sample and a 2 nm Ag film without PCBM underneath were made as references. All samples were heated at 150 °C for 10 minutes on a hot plate. To minimize degradation, the samples were transferred from our nitrogen glove box in Davis, CA, to the Advanced Light Source (ALS) synchrotron in Berkeley, CA in sealed container. X-ray absorption spectra on the carbon K-edge and were taken at beam line 6.3.1 of the Advanced Light Source synchrotron at Lawrence Berkeley National Laboratory. Spectra were acquired by total electron yield in rapid scanning mode, so that the time for a single scan from 270–320 eV was only 45 s. None of the samples showed any signs of radiation damage during the 10 scans that were averaged for improved statistics. Carbon K-edge scans over the clean Ag reference sample were used as a measure of the incident flux I_0, to avoid any artifacts from carbon contamination of the beam line. A small structure below the K-edge from second-order excitation of oxygen in the Al- and Ca-coated samples and a linear background in the K-edge region were subtracted, and the signals were normalized to unity at the energy of 310 eV above the edge.

For optical microscope measurements, the samples were fabricated by spin coating a solution of P3HT:PCBM (1:1, 20 mg/mL) in chlorobenzene and 4% nitrobenzene by volume onto glass which was previously coated with poly(3,4-ethylenedioxythiophene):poly(styrenesulfonate) (PEDOT:PSS, Clevios P VP AI 4083). Following deposition of 10 nm of metal by thermal evaporation, the samples were heated for 1 hour in a N_2 glove box. Measurements were conducted in reflection mode.

OPV devices were fabricated on etched ITO-coated glass substrates. PEDOT:PSS was spin coated to achieve a ~40 nm layer. After spin coating, the films were annealed in air at 110 °C for 5 minutes and then transferred to a nitrogen glove box. P3HT and PCBM solutions were prepared in the same manner that was used for neutron reflectometry measurements. The BHJ was spin coated from the solution in the glove box. The films were not thermally or solvent annealed prior to electrode deposition. Metal electrodes were deposited by thermal evaporation. The metal was deposited at 0.2 Å/s for the first 5 nm then the rate was increased to 1.5 Å/s. Device measurements were made under 1 Sun of simulated AM 1.5G light with no mismatch correction. A certified reference cell was used to calibrate the intensity of the solar simulator.

Acknowledgements

References

[1] G. Yu, J. Gao, J. C. Hummelen, F. Wudl, A. J. Heeger, *Science* **1995**, *270*, 1789–1791.

[2] J. J. M. Halls, C. A. Walsh, N. C. Greenham, E. A. Marseglia, R. H. Friend, S. C. Moratti, A. B. Holmes, *Nature* **1995**, *376*, 498–500.

[3] J. J. M. Halls, A. C. Arias, J. D. MacKenzie, W. S. Wu, M. Inbasekaran, E. P. Woo, R. H. Friend, *Adv. Mater.* **2000**, *12*, 498–502.

[4] H. Hoppe, N. S. Sariciftci, *J. Mater. Chem.* **2006**, *16*, 45–61.

[5] M. Campoy-Quiles, T. Ferenczi, T. Agostinelli, P. G. Etchegoin, Y. Kim, T. D. Anthopoulos, P. N. Stavrinou, D. D. C. Bradley, J. Nelson, *Nat. Mater.* **2008**, *7*, 158–164.

[6] D. S. Germack, C. K. Chan, R. J. Kline, D. A. Fischer, D. J. Gundlach, M. F. Toney, L. J. Richter, D. M. DeLongchamp, *Macromolecules* **2010**, *43*, 3828–3836.

[7] N. D. Treat, M. A. Brady, G. Smith, M. F. Toney, E. J. Kramer, C. J. Hawker, M. L. Chabinyc, *Adv. Energy Mater.* **2011**, *1*, 82–89.

[8] D. Chen, F. Liu, C. Wang, A. Nakahara, T. P. Russell, *Nano Letters* **2011**, *11*, 2071–2078.

[9] D. Chen, A. Nakahara, D. Wei, D. Nordlund, T. P. Russell, *Nano Letters* **2011**, *11*, 561–567.

[10] Z. Xu, L. M. Chen, G. W. Yang, C. H. Huang, J. H. Hou, Y. Wu, G. Li, C. S. Hsu, Y. Yang, *Adv. Funct. Mater.* **2009**, *19*, 1227–1234.

[11] A. Orimo, K. Masuda, S. Honda, H. Benten, S. Ito, H. Ohkita, H. Tsuji, *Appl. Phys. Lett.* **2010**, *96*, 043305.

[12] D. S. Germack, C. K. Chan, B. H. Hamadani, L. J. Richter, D. A. Fischer, D. J. Gundlach, D. M. DeLongchamp, *Appl. Phys. Lett.* **2009**, *94*, 233303.

[13] B. Paci, A. Generosi, V. R. Albertini, P. Perfetti, R. de Bettignies, M. Firon, J. Leroy, C. Sentein, *Appl. Phys. Lett.* **2005**, *87*, 194110.

[14] J. W. Kiel, B. J. Kirby, C. F. Majkrzak, B. B. Maranville, M. E. Mackay, *Soft Matter* **2010**, *6*, 641–646.

[15] A. J. Parnell, A. D. F. Dunbar, A. J. Pearson, P. A. Staniec, A. J. C. Dennison, H. Hamamatsu, M. W. A. Skoda, D. G. Lidzey, R. A. L. Jones, *Adv. Mater.* **2010**, *22*, 2444–2447.

[16] K. H. Lee, P. E. Schwenn, A. R. G. Smith, H. Cavaye, P. E. Shaw, M. James, K. B. Krueger, I. R. Gentle, P. Meredith, P. L. Burn, *Adv. Mater.* **2011**, *23*, 766–770.

[17] C. Rochester, S. Mauger, A. Moulé, *J. Phys. Chem. C* **2012**, *116*, 7287–7292.

[18] S. S. van Bavel, M. Barenklau, G. de With, H. Hoppe, J. Loos, *Adv. Funct. Mater.* **2010**, *20*, 1458–1463.

[19] A. Morfa, T. Barnes, A. Ferguson, D. Levi, G. Rumbles, K. Rowlen, J. van de Lagemaat, *J. Polymer Sci. B: Polymer Phys.* **2011**, *49*, 186–194.

[20] M. Theander, O. Inganäs, W. Mammo, T. Olinga, M. Svensson, M. Andersson, *J. Phys. Chem. B* **1999**, *103*, 7771–7780.

[21] K. Lee, P. Schwenn, A. Smith, H. Cavaye, P. Shaw, M. James, K. Krueger, I. Gentle, P. Meredith, P. Burn, *Adv. Mater.* **2011**, *23*, 766–770.

[22] J. Higgins, H. Benoît, *Polymers and Neutron Scattering*, Oxford: Clarendon Press, **1994**.

[23] M. Dubey, M. S. Jablin, P. Wang, M. Mocko, J. Majewski, *Eur. Phys. J. Plus* **2011**, *126*, 110.

[24] A. Moulé, K. Meerholz, *Adv. Funct. Mater.* **2009**, *19*, 3028–3036.

[25] A. J. Moulé, K. Meerholz, *Adv. Mater.* **2008**, *20*, 240–245.

[26] H. Wang, E. Gomez, J. Kim, Z. Guan, C. Jaye, D. Fisher, A. Kahn, Y. Loo, *Chem. Mater.* **2011**, *23*, 2020–2023.

[27] N. I. of Standards and Technology (NIST) Center for Neutron Research, *Scattering Length Density Calculator*, http://www.ncnr.nist.gov/resources/sldcalc.html, Accessed September 2011.

[28] F. Padinger, R. S. Rittberger, N. S. Sariciftci, *Adv. Funct. Mater.* **2003**, *13*, 85–88.

[29] W. Ma, C. Yang, X. Gong, K. Lee, A. J. Heeger, *Adv. Funct. Mater.* **2005**, *15*, 1617–1622.

[30] J. Zhao, A. Swinnen, G. Van Assche, J. Manca, D. Vanderzande, B. Van Mele, *J. Phys. Chem. B* **2009**, *113*, 1587–1591.

[31] C. M. Bjorstrom, A. Bernasik, J. Rysz, A. Budkowski, S. Nilsson, M. Svensson, M. R. Andersson, K. O. Magnusson, E. Moons, *J. Phys.: Condens. Matter* **2005**, *17*, L529–L534.

[32] X. J. Wang, T. Ederth, O. Inganas, *Langmuir* **2006**, *22*, 9287–9294.

[33] J. Y. Kim, D. Frisbie, *J. Phys. Chem. C* **2008**, *112*, 17726–17736.

[34] C. Müller, T. A. M. Ferenczi, M. Campoy-Quiles, J. M. Frost, D. D. C. Bradley, P. Smith, N. Stingelin-Stutzmann, J. Nelson, *Adv. Mater.* **2008**, *20*, 3510–3515.

[35] L. Vitos, A. V. Ruban, H. L. Skriver, J. Kollar, *Surf. Sci.* **1998**, *411*, 186–202.

[36] L. Chang, H. W. A. Lademann, J.-B. Bonekamp, K. Meerholz, A. J. Moulé, *Adv. Funct. Mater.* **2011**, *21*, 1779–1787.

[37] A. Tillack, K. Nonne, N. D. MacLeod, B.A., K. Nagle, J. Bradley, S. Hau, H.-L. Yup, G. Jen, A.K.-Y. Seidler, G. D.S., *ACS Appl. Mater. Interfaces* **2011**, *3*, 726–732.

[38] A. Anselmo, L. Lindgren, J. Rysz, A. Bernasik, A. Budkowski, M. Andersson, K. Svensson, J. van Stam, E. Moons, *Chem. Mater.* **2011**, *23*, 2295–2302.

[39] K. Walzer, B. Maennig, M. Pfeiffer, K. Leo, *Chem. Rev.* **2007**, *107*, 1233–1271.

[40] C. Press in *CRC Handbook of Chemistry and Physics* (Ed.: W. Haynes), CRC Press/Taylor and Francis, Boca Raton, FL, 91st ed., **2011**, p. 114.

[41] M. C. Scharber, D. Wuhlbacher, M. Koppe, P. Denk, C. Waldauf, A. J. Heeger, C. L. Brabec, *Adv. Mater.* **2006**, *18*, 789–794.

[42] P. Sehati, S. Braun, L. Lindell, X. Liu, L. Andersson, F. M, *IEEE J. Selected Topics in Quantum Electronics* **2010**, *16*, 1718–1724.

[43] L. Forró, L. Mihály, *Rep. Prog. Phys.* **2001**, *64*, 649–699.

[44] S. Friedrich, O. B. Drury, S. J. George, S. P. Cramer, *Nucl. Instrum. Methods Phys. Res. Sect. A* **2007**, *582*, 187–189.

[45] M. P. de Jong, L. J. van Ijzendoorn, M. J. A. de Voigt, *Appl. Phys. Lett.* **2000**, *77*, 2255–2257.

[46] F. C. Krebs, K. Norrman, *Prog. Photovoltaics: Res. Appl.* **2007**, *15*, 697–712.

[47] S. J. Naftel, T. K. Sham, Y. M. Yiu, B. W. Yates, *J. Synchrotron Radiat.* **2001**, *8*, 255–257.

[48] A. Moulé, K. Meerholz, *Appl. Phys. B* **2007**, *86*, 771–777.

[49] D. M. Huang, S. A. Mauger, S. Friedrich, S. J. George, D. Dumitriu-LaGrange, S. Yoon, A. J. Moulé, *Adv. Funct. Mater.* **2011**, *21*, 1657–1665.

[50] B. P. Lyons, N. Clarke, C. Groves, *J. Phys. Chem. C* **2011**, *115*, 22572–22577.

[51] A. Maurano, R. Hamilton, C. Shuttle, A. Ballantyne, J. Nelson, B. O'Regan, W. Zhang, I. McCulloch, H. Azimi, M. Morana, C. J. Brabec, J. Durrant, *Adv. Mater.* **2010**, *22*, 4987–4992.

[52] W. Ma, C. Yang, X. Gong, K. Lee, A. J. Heeger, *Adv. Funct. Mater.* **2005**, *15*, 1617–1622.

[53] P. A. Kienzle, J. Krycka, N. Patel, I. Sahin, *Refl1D software suite (Version 0.6.19)*, http://reflectometry.org/danse.

Supporting Information for "Self assembly of selective interfaces in organic photovoltaics"

Scott A. Mauger   Lilian Chang   Stephan Friedrich
Christopher W. Rochester   David M. Huang
Peng Wang Adam J. Moulé

September 10, 2012

Table S1: Roughness (σ) for top of BHJ, Al, and AlOx. The roughness of the BHJ, σ_{BHJ}, was varied systematically and fixed for fitting while the other roughness values, σ_{Al} and σ_{AlOx} were fit along with the layer thicknesses to minimize the χ^2 error. The values in the first row are the best fit achieved, when all roughness values were allowed to vary.

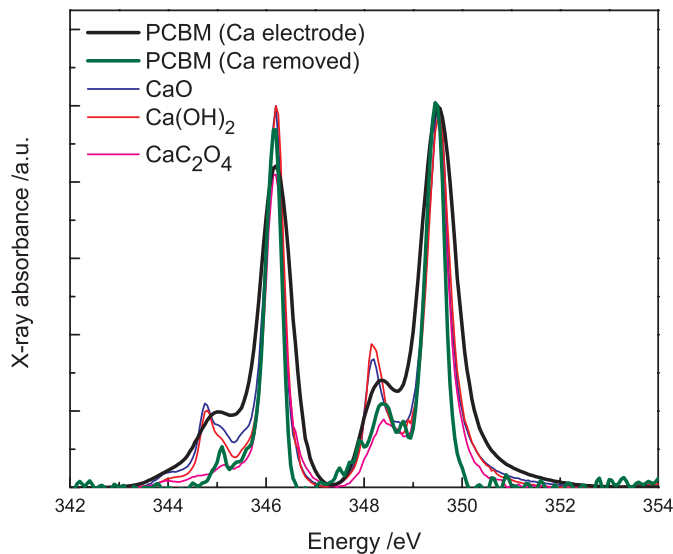| σ_{BHJ} (Å)	σ_{Al} (Å)	σ_{AlOx} (Å)	χ^2
0.5003	8.113	11.03	23.740
2.0	7.89	10.70	23.75
5.0	7.69	10.70	23.763
10.0	8.11	10.28	23.804
15.0	8.45	9.39	23.879
20.0	6.55	9.08	23.963

Figure S1: Near edge x-ray absorption fine structure (NEXAFS) of the Ca L-edge. NEXAFS by total electron yield (TEY) on PCBM film with a Ca capping layer of Ca (—) and by partial fluorescence yield (PFY) a PCBM film with the Ca layer removed prior to measurement (—). TEY spectra of commercial model compounds CaO (—), Ca(OH)$_2$ (—) and CaC$_2$O$_4$ (—) are included for comparison